Available online at www.eccomasproceedia.org
Eccomas Proceedia COMPDYN (2023) 1707-1718

ECCOMAS
Proceedia

COMPDYN 2023
9th ECCOMAS Thematic Conference on
Computational Methods in Structural Dynamics and Earthquake Engineering
M. Papadrakakis, M. Fragiadakis (eds.)
Athens, Greece, 12-14 June 2023

NONLINEAR BEHAVIOR OF EXISTING MASONRY STRUCTURES: AN APPLICATION TO A CASE STUDY WITH DIFFERENT STRUCTURAL CONFIGURATIONS

Roselena Sulla[1], Michele D'Amato[1], Rosario Gigliotti[2], and Domenico Liberatore[3]

[1] DiCEM, Dept. of European and Mediterranean Cultures: Architecture, Environment and Cultural Heritage, University of Basilicata
Via Lanera, Matera 75100, Italy
e-mail: {roselena.sulla,michele.damato}@unibas.it

[2] DISG, Dept. of Structural and Geotechnical Engineering, Sapienza University of Rome
Via Eudossiana 18, Rome 00184, Italy
e-mail: rosario.gigliotti@uniroma1.it

[3] DSDRA, Dept. of History, Representation and Restoration of Architecture, Sapienza University of Rome
Piazza Borghese 9, Rome 00186, Italy
e-mail: domenico.liberatore@uniroma1.it

Abstract

Numerical simulations and computational methods are directly connected to structures strength models and modeling criteria. This work refers to masonry elements, in particular to the piers and spandrels strength models according to the Italian Design Code. These models are firstly reviewed in a dimensionless form, then applied to a parametric analysis comparing the results obtained by varying masonry strength and in-plane floor flexibility. The masonry buildings seismic behavior is analyzed by performing pushover analyses according to the equivalent frame model on an ideal case study, which is replicated with the same geometric and dimensional characteristics but with different masonry types and floor behaviors. The aim is to evaluate the influence of masonry strength and floor stiffness on the global response. Finally, fragility curves are derived and compared to literature ones.

Keywords: Existing Masonry Structures, Fragility Curves, Numerical Methods, Pushover Analysis, Seismic Behavior, Strength Models.

ISSN:2623-3347
Peer-review under responsibility of the organizing committee of COMPDYN 2023.
doi: 10.7712/120123.10513.20744

1 INTRODUCTION

A significant part of the architectural heritage that characterizes the Italian territory includes buildings having a masonry structure of different types (e.g., brick masonry, stone masonry, etc.), and each of them corresponds to a different compressive strength. In particular, the masonry type, as well as the floor stiffness, could affect the constructions response to seismic action. This behavior could be assessed through several numerical methods: one example is presented in [1], where an existing brick masonry church is considered as a case study on which apply the linear kinematic analysis to evaluate the failure mechanisms activation regarding the macro-elements constituting the church. On the other hand, the seismic behavior of masonry structures could be assessed through nonlinear analyses (e.g. pushover analysis) taking into account the equivalent frame model: according to this modeling criterion, the main elements constituting a masonry structure are piers and spandrels. Many studies in literature consider this method. Among the others, in [2] a quantitative assessment concerns the effect of modeling uncertainties on the seismic response of masonry buildings, investigated through nonlinear static analyses and equivalent frame model; in [3] a review about the uses and limits of the equivalent frame model is presented. Furthermore, to define the probability of reaching a certain damage level, fragility curves may be derived from a numerical model or by observational basis, as in [4] and in [5].

The aim of this study is to investigate the strength models of masonry elements, in accordance with the Italian Design Code [6] and its Instructions [7], by considering a reference ideal case study and varying masonry type and floor type (i.e. masonry strength and in-plane floor stiffness). Therefore, to evaluate its seismic behavior, a parametric pushover analysis is conducted and fragility curves are derived, whose results are presented and discussed below.

2 STRENGTH MODELS: REVIEW AND DISCUSSION

In accordance with [7], geometry, boundary conditions, structural function and masonry type represent the factors affecting the capacity models of masonry elements. The elements constituting a masonry structure are mainly of two types, depending on their axis:

- Piers: masonry elements characterized by vertical axis and which may be affected by three main types of failure, namely bending, shear sliding and shear with diagonal cracking;
- Spandrels: in contrast to masonry piers, they present a horizontal axis, and the potential in-plane failure mechanisms involving them are bending and shear with diagonal cracking.

The Italian Design Code [6] and its Instructions [7] provide relations evaluating the strength of these failure mechanisms, that are reported in the following sections. In addition, they are reviewed in a dimensionless form, to be subsequently applied to a case study, whose response is then investigated through pushover analysis (as it is possible to note also in [8]).

2.1 Pier bending

As regards the pier bending, in accordance with [6] the ultimate resistant moment is derived by the following equation, expressing the relation between the axial load and the bending moment:

$$M_u = \left(l^2\, t\, \frac{\sigma_0}{2}\right)\left(1 - \frac{\sigma_0}{0.85 f_d}\right) \tag{1}$$

It is possible to define the dimensionless normal stress, ranging between 0 and 1:

$$\alpha = \sigma_0 / 0.85 f_d \tag{2}$$

Then, we obtain:

$$\frac{M_u}{l^2\ t\ 0.85 f_d} = \frac{\alpha}{2}(1-\alpha) \tag{3}$$

M_u is the moment corresponding to bending failure; l is the masonry pier total length; t is the thickness of the compressed area of the pier; $\sigma_0 = N/(l\ t)$ is the mean normal stress, referred to the section total area; N is the design axial force, positive if compressive (if N is tensile, $M_u = 0$); $f_d = f/CF$ is the masonry design compressive strength; f is the masonry mean compressive strength; CF is the Confidence Factor, depending on the Knowledge Level.

Therefore, Eq. (1) allows to represent, in a dimensionless form, the interaction domain between axial load and bending moment. This interaction domain does not depend on masonry type, pier thickness and length (Figure 1); it should be noted that it starts from the origin (tensile strength is taken equal to zero), while the maximum flexural strength is achieved when the dimensionless normal stress takes the value $\alpha = 0.5$.

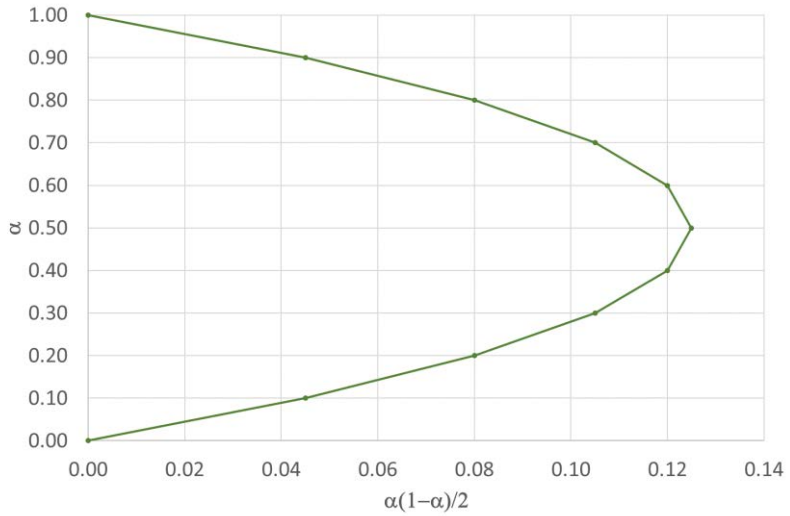

Figure 1: Masonry pier interaction domain.

2.2 Pier shear sliding

As concerns the pier shear sliding verification, [6] provides the following relation to assess the structural element shear capacity:

$$V_t = l'\ t\ f_{vd}$$

$$f_{vd} = \frac{f_{v0}}{CF} + 0.4\ \sigma_n \leq f_{V,lim} \tag{4}$$

$$f_{V,lim} = \frac{0.065 f_b}{0.7}$$

where: l' is the masonry pier compressed part length, defined with reference to a compression linear diagram and no tensile strength; t is the masonry pier thickness; f_{vd} is the masonry design shear strength; f_{v0} is the mean shear strength in the absence of normal stresses; $\sigma_n = N/(l't)$ is the mean normal stress calculated on the compressed part of the cross section; $f_{V,lim}$ represents the limitation on block cracking, obtained for standard shape blocks; f_b is the block normalized compressive strength.

One may note that, in this case, the strength depends on the length of the compressed part l', where the shear strength takes place. Hence, Eq. (4) could be converted in a dimensionless relation, considering a linear distribution of the normal stress acting on *l'*:

$$\frac{V_t}{l\ t\ f_{V,lim}} = \frac{\tau_{lim}}{f_{V,lim}} = 3\left(\frac{1}{2} - \frac{e}{l}\right) \tag{5}$$

In the previous equation: τ_{lim} is the mean shear strength (calculated referring to the pier total length *l*); e is the eccentricity, that is the distance between the pier axis and the compressive force, ranging between 0 and the masonry pier half-length $l/2$, and the ratio e/l ranges between 0 and 0.5. It is clear to observe that the shear strength is linearly dependent on the ratio e/l, varying in a range between 1.5 (when e/l = 0, i.e. when only axial load is applied) and 0 (when e/l = 0.5, i.e. when the eccentricity e is equal to $l/2$). This linear relation, independent from any parameter referring to masonry type and element geometry, is shown in Figure 2.

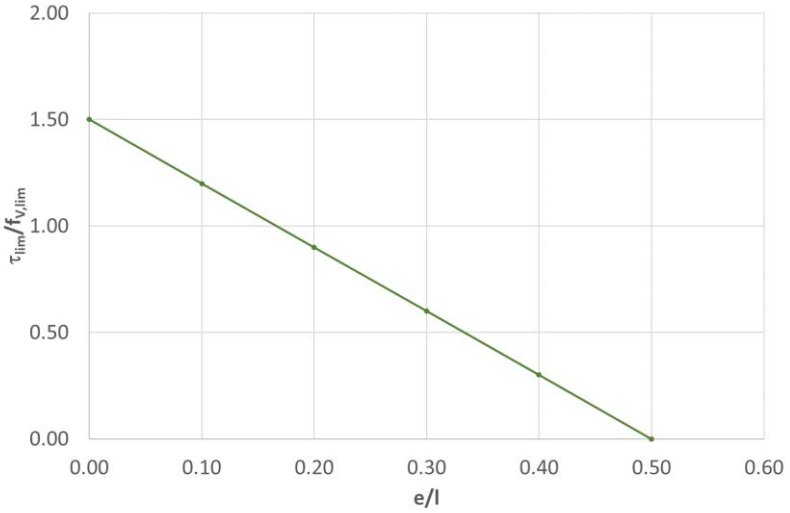

Figure 2: Shear strength on the pier section.

2.3 Spandrel bending

In accordance with [6], the same strength model adopted for masonry piers should be taken in consideration when the axial force is known. On the contrary, if the axial force is unknown, and there are horizontal elements in tension (e.g. steel tie-rods, reinforced concrete ring beams), the spandrels ultimate bending strength may be expressed as follows:

$$M_u = H_p\ \frac{h}{2}\left(1 - \frac{H_p}{0.85 \cdot f_{hd} \cdot h \cdot t}\right) \tag{6}$$

Also in this case, Eq. (6) may be converted in dimensionless form defining:

$$\beta = H_p / 0.85 f_{hd} h t \tag{7}$$

which provides:

$$\frac{M_u}{h^2\ t\ 0.85 f_{hd}} = \frac{\beta}{2}(1 - \beta) \tag{8}$$

H_p is the minimum between the tensile capacity of the horizontal element and $0.4 f_{hd} h t$; f_{hd} is the masonry design compressive strength along the horizontal direction; h is the cross section height of the spandrel.

Eq. (8) is truncated when $H_p = 0.4 f_{hd} ht$, i.e. when the value $\beta^* \approx 0.47$ is reached (Figure 3).

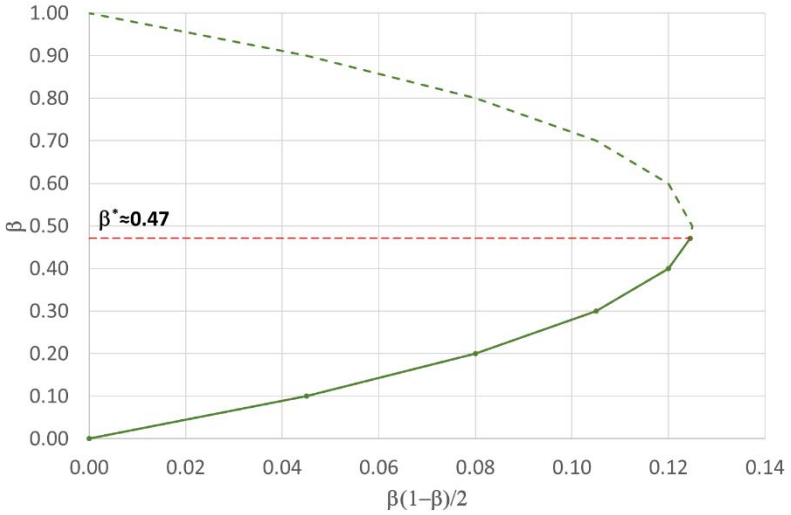

Figure 3: Analytic relationship reported in Eq. (8).

2.4 Pier and spandrel shear strength with diagonal cracking

Before evaluating the shear strength with diagonal cracking, both in masonry piers and spandrels, [7] defines two groups for the shear assessment with reference to the masonry fabric, i.e. masonry with irregular fabric and masonry with regular fabric.

As regards masonry with irregular fabric, the shear for in-plane actions may be calculated as follows:

$$V_t = l\, t \frac{1.5\, \tau_{0d}}{b} \sqrt{1 + \frac{\sigma_0}{1.5\, \tau_{0d}}} = l\, t \frac{f_{td}}{b} \sqrt{1 + \frac{\sigma_0}{f_{td}}} \tag{9}$$

Considering the ratio between the normal stress and the diagonal tensile strength:

$$\gamma = \sigma_0 / f_{td} \tag{10}$$

with $\gamma \geq 0$, the following dimensionless equation may be obtained:

$$\frac{V_t}{l\, t\, f_{td}} = \frac{\tau}{f_{td}} = \frac{1}{b} \sqrt{1 + \gamma} \tag{11}$$

where: f_{td} and τ_{0d} are the diagonal cracking tensile strength and the corresponding masonry reference shear strength, respectively; $b = h/l$ is a correction coefficient depending on the panel aspect ratio related to the stress distribution on the cross section ($1 \leq b \leq 1.5$); h is the panel height.

As far as masonry with regular fabric is concerned, it is possible to apply Eq. (9) to assess the shear strength, considering a simplified approach. Otherwise, the following equation should be considered:

$$\begin{aligned} V_t &= \frac{lt}{b(1+\mu\varphi)} (f_{v0d} + \mu\sigma_0) \leq V_{t,lim} \\ V_{t,lim} &= \frac{lt}{b} \frac{f_{btd}}{2.3} \sqrt{1 + \frac{\sigma_0}{f_{btd}}} \end{aligned} \tag{12}$$

where: f_{v0d} is the masonry shear strength; μ is the friction coefficient; φ is the interlocking coefficient (i.e. the ratio of the block height to the minimum overlapping length of two units belonging to two consecutive joints); $V_{t,lim}$ is a limit value that can be approximated as function of the blocks tensile failure f_{btd}, and taking into account the panel geometry.

In this case, assuming the ratio of normal stress to the block tensile failure:

$$\delta = \sigma_0 / f_{btd} \tag{13}$$

the following dimensionless equation, where $\delta \geq 0$, is derived:

$$2.3 \frac{V_{t,lim}}{l\, t\, f_{btd}} = 2.3 \frac{\tau_{lim}}{f_{btd}} = \frac{1}{b}\sqrt{1+\delta} \tag{14}$$

It should be noted that, as presented in Figure 4, as γ (δ) increases, the mean shear strength τ (τ_{lim}) increases. In addition, there is an upper bound, represented by the light green curve (i.e. with b = 1), and a lower bound, that is the dark green curve (i.e. with b = 1.5), since this equation is affected by the element aspect ratio and the element dimensions.

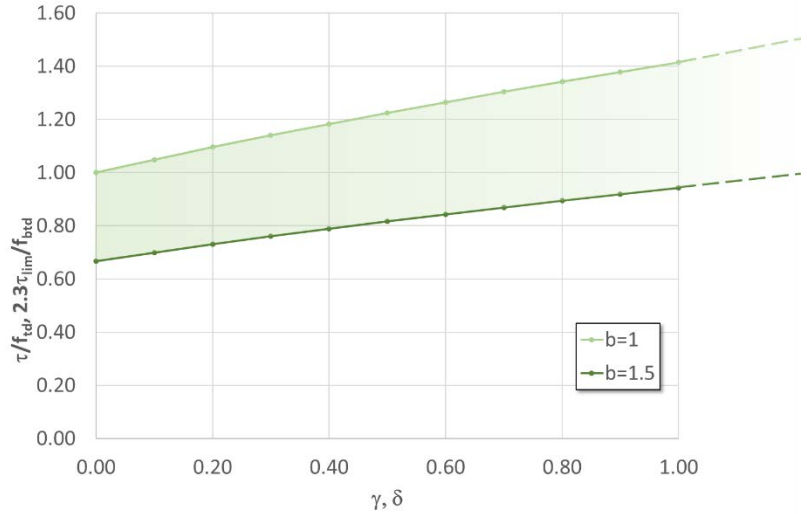

Figure 4: Pier/spandrel shear strength for irregular and regular masonry.

3 NUMERICAL ANALYSES ON A CASE STUDY

To validate some of the strength models in dimensionless form, previously discussed, and to evaluate the global seismic response of a masonry building, an ideal case study, with nominal life V_N = 50 years and class of use II, is considered (Figure 5). It reproduces a typical existing masonry structure having a simple configuration. The structure is characterized by three stories, with wall thickness equal to 60 cm. The assumed Confidence Factor is CF = 1.2, corresponding to an extensive Knowledge Level [7]. Moreover, the assumed location is Salerno (Italy), with soil class C and topographic category T1.

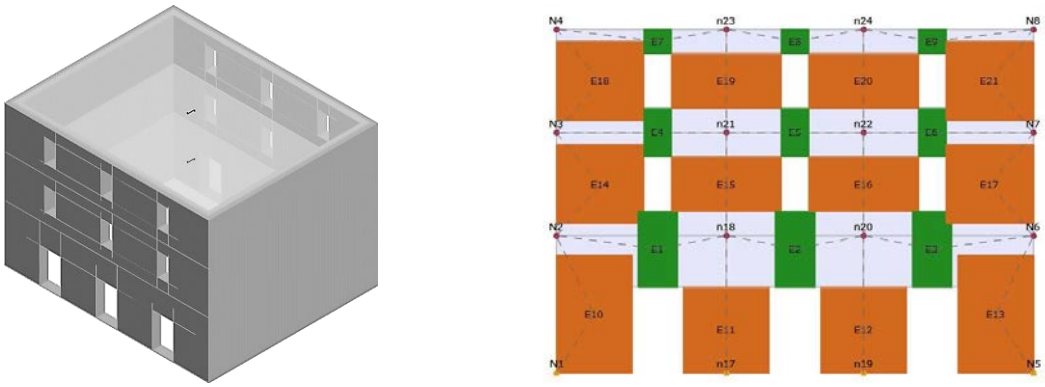

a) b)

Figure 5: a) Case study 3D view and b) equivalent frame model with orange piers and green spandrels (3Muri Professional [9]).

The aim of this work is to investigate the in-plane failure mechanisms involving masonry piers and spandrels constituting the reference masonry wall. Thereby, parametric pushover analyses are performed, using the software 3Muri Professional (www.stadata.it [9]), considering the combination of three different masonry types and three different floor types, obtaining as a result nine cases to be analyzed. Below, the masonry types considered, with increasing mechanical properties whose assumed values refer to [7], are reported:

- Irregular Stone Masonry (ISM);
- Regular Stone Masonry (RSM);
- Brick Masonry (BM).

The three floor types taken into account, with decreasing in-plane stiffness, are the following:

- Rigid Floor (RF);
- Semi-Rigid Floor (SRF);
- Flexible Floor (FF).

3.1 Strength models

The strength models of bending and shear with diagonal cracking are adopted for the piers constituting the reference masonry wall (Figure 5b). Before discussing the results of the pushover analyses, two limit cases are considered: ISM with FF, and BM with RF. As regards pier bending, the dimensionless normal stress α ranges between 0.02 and 0.34 in the first case, and between 0.02 and 0.20 in the second case (yellow and red rhombuses, respectively, in Figure 6). Conversely, as concerns the pier shear with diagonal cracking, one may note that the differences of γ (δ) between the two cases are more evident, and the dots are located on the limit curves, depending on the element dimensions.

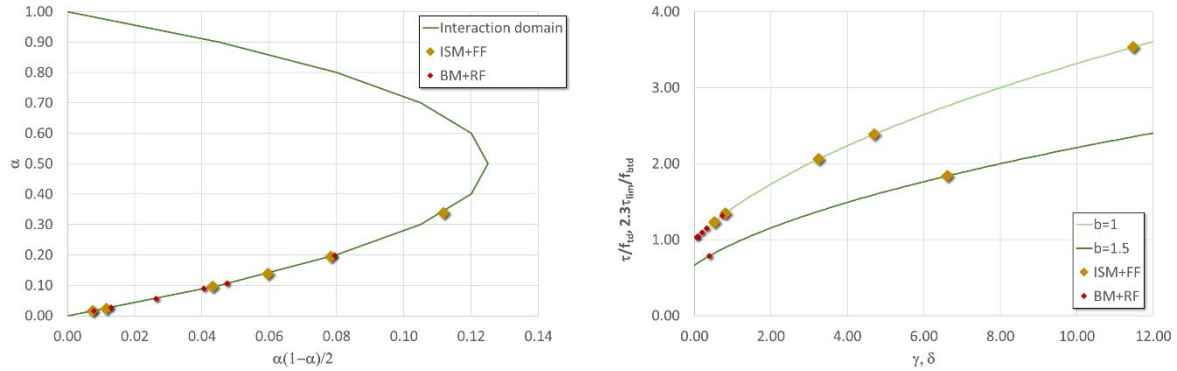

a) b)

Figure 6: a) Masonry pier bending interaction domain and b) shear strength.

3.2 Pushover analyses

The pushover analyses are conducted along the +X direction, considering a static force distribution and no load eccentricity. The in-plane failure mechanisms involving the reference masonry wall piers and spandrels are shown in Figure 7. In all the cases analyzed (i.e. by varying masonry and floor type in terms of mechanical properties and in-plane stiffness, respectively), a mixed failure mechanism may be detected: bending failure involves spandrels at all floors, the ground floor piers present mainly bending failure, some upper floors piers fail in bending and in shear.

Figure 7: Piers and spandrels mechanisms comparisons (3Muri Professional [9]).

As concerns the pushover curves (Figure 8), it should be noted that the most evident differences by varying the in-plane floor stiffness refer to BM and RSM, while irrelevant ones are found for ISM (i.e. the case of low-strength masonry). Therefore, the masonry strength is the principal variable affecting this case study response.

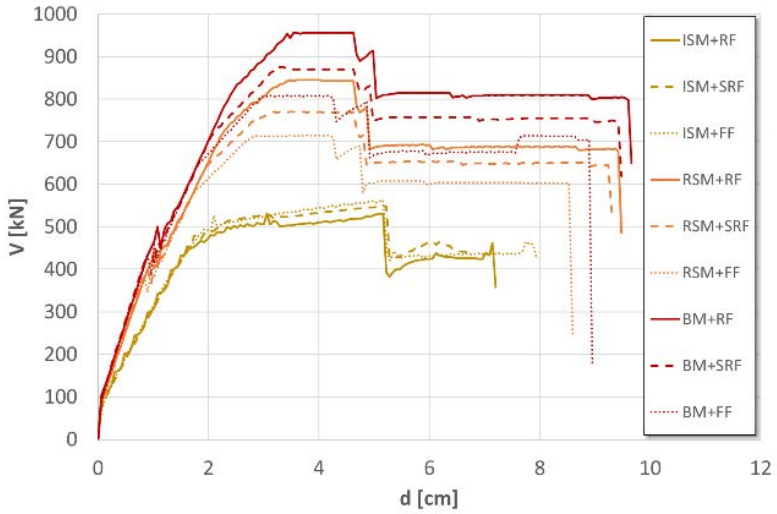

Figure 8: Pushover curves.

3.3 Fragility curves

For the fragility curves definition, this work refers to [10]. In general, a fragility function is a mathematical function representing the probability of occurrence of an event depending on an environmental excitation measure (e.g. acceleration). In other words, a fragility function may be defined as the cumulative distribution function of an asset capacity to be able to withstand a specific limit state. In the present case, it represents the probability of reaching a damage level equal or greater than a specific damage level (or limit state).

Starting from the Capacity Peak Ground Accelerations (PGA_C) resulting for each of the nine cases considered, related to Damage Limit State (DLS) and Life-Safety Limit State (LSLS), the fragility curves are derived according to the following method.

A standard normal function is considered to define the parameter p the fragility curves depend on, then a binomial function is applied to derive the probability $P(k) = P_{LS,i}$ of achieving a damage level k, as described in [11], [12] and [13]:

$$p = \Phi\left(\frac{ln(IM/\vartheta)}{\beta}\right)$$
$$P(k) = \binom{n}{k} p^k (1-p)^{n-k} \tag{15}$$

where: IM is an Intensity Measure, in this case equal to the Peak Ground Acceleration (PGA); ϑ is the median; β is the logarithmic standard deviation; n is the maximum damage level (n = 5, according to the EMS-98 scale [14]); k represents the damage level ranging between 0 and 5 (in this study, it is assumed k = 2 as DLS and k = 3 as LSLS). Finally, the maximum likelihood estimation is applied as follows, with m = 9 (i.e. the number of analyses performed in this study):

$$L(\vartheta, \beta) = \prod_{i=1}^{m} P_{DLS,i} \prod_{i=1}^{m} P_{LSLS,i} \tag{16}$$

In this way, the values $\hat{\vartheta}$ and $\hat{\beta}$ which maximize the likelihood are obtained and used to derive, through the binomial function, the probability $P(D = D_k)$, where D is an uncertain damage level and D_k is a specific damage level, with k = 0, …, 5, then the probability damage curves (Figure 9a) and, finally, the fragility curves (Figure 9b) with the equation [15]:

$$\sum_{i=k}^{n} P(D = D_k) = P(D \geq D_k) \tag{17}$$

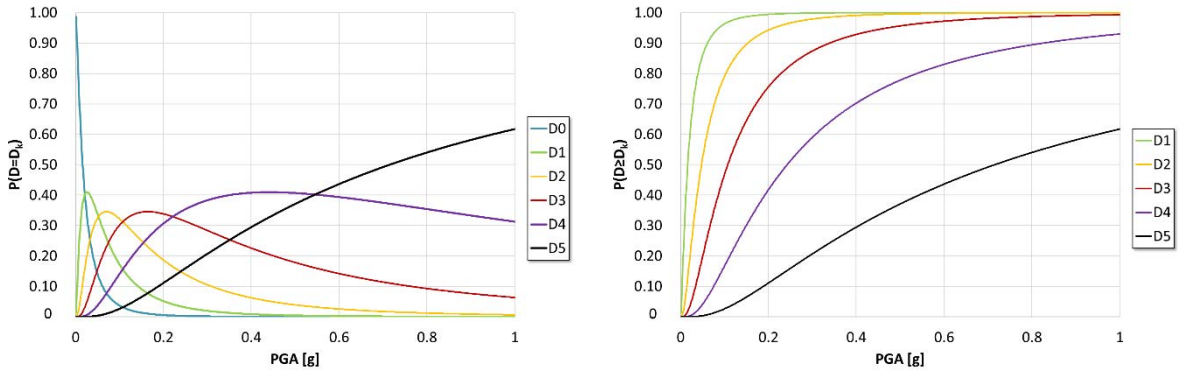

a) b)

Figure 9: a) Probability damage curves and b) fragility curves.

The fragility curves obtained are then compared with the ones presented in [4], where Classes A, B and C1 represent the vulnerability classes according to Da.D.O. [16]. This comparison is shown in Figure 10, demonstrating a substantially similar trend between the curves plotted, even though the fragility curves here derived are more prudential than the literature ones. In fact, for the same PGA value, they show a higher damage probability. It should be remarked that they are derived starting from a small analyses sample including different masonry and floor types.

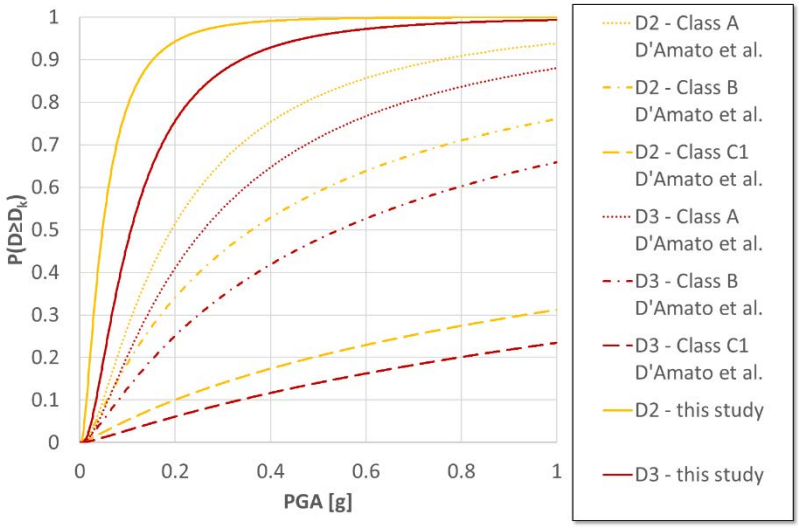

Figure 10: Comparison between [4] and this study.

4 CONCLUSIONS

In this study parametric analyses have been performed, aimed at defining a methodological approach for the proposal of mechanical fragility curves. To this scope, a case study has been considered, reproducing an existing masonry building having three floors with different masonry and floor types.

The numerical analyses conducted highlight that the lateral response is mainly affected by masonry strength. Moreover, in the case of low-strength masonry, the in-plane floor stiffness provides a low influence on the global response.

The failure mechanisms obtained mainly refer, in the cases analyzed, to bending moment, occurring at all levels both in piers and spandrels. In addition, the global failure is distributed over the masonry wall, even though there are some undamaged piers on the upper stories.

Finally, the preliminary fragility curves obtained seem to be more conservative than the other ones considered for comparison in this study. In the future, an extension of the parametric study should be conducted in order to improve and validate the reliability of the approach proposed that can be extended to other building typologies.

REFERENCES

[1] M. D'Amato, R. Sulla, Investigations of masonry churches seismic performance with numerical models: application to a case study. *Archives of Civil and Mechanical Engineering,* **21**, 161, 2021. https://doi.org/10.1007/s43452-021-00312-5

[2] S. Bracchi, M. Rota, A. Penna, G. Magenes, Consideration of modelling uncertainties in the seismic assessment of masonry buildings by equivalent-frame approach. *Bulletin of Earthquake Engineering,* **13**, 3423-3448, 2015. https://doi.org/10.1007/s10518-015-9760-z

[3] E. Quagliarini, G. Maracchini, F. Clementi, Uses and limits of the Equivalent Frame Model on existing unreinforced masonry buildings for assessing their seismic risk: A review. *Journal of Building Engineering,* **10**, 166-182, 2017. http://dx.doi.org/10.1016/j.jobe.2017.03.004

[4] M. D'Amato, R. Laguardia, G. Di Trocchio, M. Coltellacci, R. Gigliotti, Seismic Risk Assessment for Masonry Buildings Typologies from L'Aquila 2009 Earthquake Damage Data. *Journal of Earthquake Engineering,* **26**, 9, 4545-4579, 2022. https://doi.org/10.1080/13632469.2020.1835750

[5] M. Tatangelo, L. Audisio, M. D'Amato, R. Gigliotti, Seismic risk analysis on masonry buildings damaged by L'Aquila 2009 and Emilia 2012 earthquakes. *Procedia Structural Integrity,* **44**, 990-997, 2023. https://doi.org/10.1016/j.prostr.2023.01.128

[6] *Italian Design Code, Ministerial Decree M.D. (17/01/2018)*. Aggiornamento delle "Norme Tecniche per le costruzioni" (in Italian). Rome, Italy: Italian Ministry of Infrastructure and Transportation, 2018.

[7] *Instructions for the application of the Italian Design Code M.D. (17/01/2018)*. Istruzioni per l'applicazione dell'«Aggiornamento delle "Norme tecniche per le costruzioni"» di cui al D.M. 17 gennaio 2018 (in Italian). Rome, Italy: Italian Ministry of Infrastructure and Transportation, 2019.

[8] R. Sulla, M. D'Amato, R. Gigliotti, D. Liberatore, Modeling criteria for the seismic assessment of existing masonry buildings. *Procedia Structural Integrity,* **44**, 998-1005, 2023. https://doi.org/10.1016/j.prostr.2023.01.129

[9] 3Muri, *User manual*. www.stadata.it.

[10] K. Porter, *A Beginner's Guide to Fragility, Vulnerability, and Risk*. University of Colorado Boulder, 2021. https://www.sparisk.com/pubs/Porter-beginners-guide.pdf

[11] F. Braga, M. Dolce, D. Liberatore, A statistical study on damaged buildings and an ensuing review of MSK-76 Scale. *Proceedings of the 7th European Conference on Earthquake Engineering*, Athens, 1982.

[12] S. Lagomarsino, S. Podestà, Seismic vulnerability of ancient churches. Part 2: Statistical analysis of surveyed data and methods for risk analysis. *Earthquake Spectra,* **20**, 2, 395-412, 2004b. doi: 10.1193/1.1737736

[13] D. Díaz Fuentes, P. A. Baquedano Julià, M. D'Amato, M. Laterza, Preliminary Seismic Damage Assessment of Mexican Churches after September 2017 Earthquakes. *International Journal of Architectural Heritage,* **15**, 4, 505-525, 2021. doi: 10.1080/15583058.2019.1628323

[14] G. Grunthal, *European macroseismic scale*. Luxembourg: European Seismological Commission (ESC), 1998.

[15] A. Marotta, D. Liberatore, L. Sorrentino, Development of parametric seismic fragility curves for historical churches. *Bulletin of Earthquake Engineering,* **19**, 5609-5641, 2021. https://doi.org/10.1007/s10518-021-01174-1

[16] DPC. Dipartimento della Protezione Civile, *Piattaforma Da.D.O. Database Danno Osservato - Manuale utente*. Manuale realizzato da EUCENTRE nell'ambito della Convenzione DPC-RELUIS 2015 - Progetto Operativo S3.10 ("Sviluppo e Gestione di una Piattaforma WebGIS per il Monitoraggio degli interventi su edifici privati di cui all'art.2, comma 1 lettera c) delle Ordinanze in attuazione all'art. 11 del D.L. 28/ 04/2009"). Allegato S3.10_A. Pavia, Italy, 2015.